Electronic Supplementary Material (ESI) for Nanoscale.

Supporting Information

Implanted Paramagnetic Metallofullerene Probe within Metal−Organic Framework

Haibing Meng[a,b], *Chong Zhao*[a,b], *Yongjian Li*[a,b], *Mingzhe Nie*[a,b], *Chunru Wang*[*a] *and Taishan Wang*[*a]

[a]Beijing National Laboratory for Molecular Sciences, Key Laboratory of Molecular Nanostructure and Nanotechnology, Institute of Chemistry, Chinese Academy of Sciences, Beijing 100190, China

[b]University of Chinese Academy of Sciences, Beijing 100049, China

*E-mail: wangtais@iccas.ac.cn; crwang@iccas.ac.cn

Table of Contents

1. Synthesis and Experimental Methods

1.1 General

N,N-diethylformamide (DEF, > 99%), carbon disulfide (CS_2, > 99%), Zinc nitrate hexahydrate (> 99%), 1,3,5-Tri(4-carboxyphenyl)benzene (H_3BTB, > 99%), 4-hydroxy-2,2,6,6-tetramethyl-piperidinooxy and toluene (HPLC grade) were purchased from Sigma-Aldrich. Graphite rod (spectral purity) and Sc/Ni alloy (> 99%) were purchased from General Research Institute for Nonferrous Metals (Beijing, China). All compounds were used as received.

1.2 The synthesis and purification of $Sc_3C_2@C_{80}$

The $Sc_3C_2@C_{80}$ was synthesized by arc-discharging method[1, 2]. In general, the mixture of graphite powder and Sc/Ni alloy with a mass ratio of 1:3 was filled with core-drilled graphite rods. Then the filled rods were vaporized in a Kratschmer-Huffman generator under an atmosphere of 200 Torr He. The resulted soot was Soxlet-extracted with toluene for 24 h to get fullerenes in toluene. $Sc_3C_2@C_{80}$ was isolated and purified by multi-step high performance liquid chromatography (HPLC). Figure S1 shows the HPLC and MALDI-TOF MS profiles of purified $Sc_3C_2@C_{80}$.

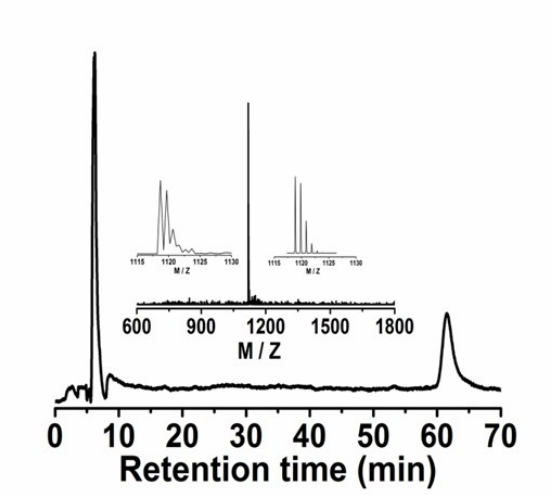

Figure S1. Chromatogram of the isolated $Sc_3C_2@C_{80}$ (20×250 mm Buckyprep column; flow rate 12 mL/min; toluene as eluent) and inset shows the MALDI-TOF MS profile of $Sc_3C_2@C_{80}$.

2. EPR measurements

The EPR experiments were carried out in Bruker E500 system. The EPR spectrum of $Sc_3C_2@C_{80}$ at room temperature shows a highly symmetric 22 lines in toluene solution

(Figure S2).

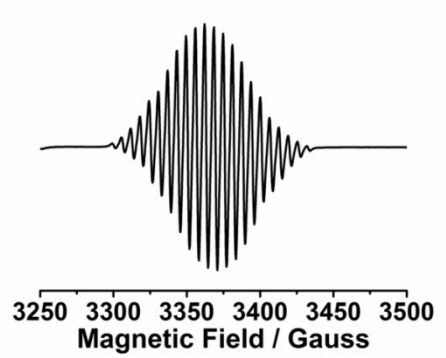

Figure S2. EPR spectrum of $Sc_3C_2@C_{80}$ in toluene at room temperature.

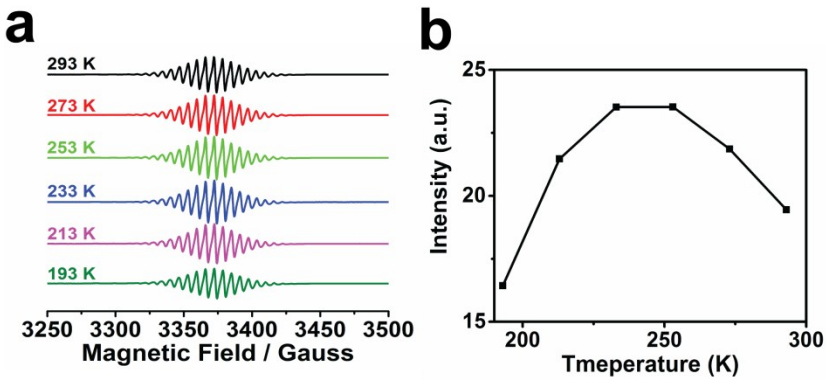

Figure S3. Temperature-dependent EPR spectra of $Sc_3C_2@C_{80}$ in $Sc_3N@C_{80}$ (1 mol%) (a). Temperature-dependent EPR peaks intensity of $Sc_3C_2@C_{80}$ in $Sc_3N@C_{80}$ (1 mol%) (b).

Temperature-dependent EPR spectra and temperature-dependent EPR peaks intensity of $Sc_3C_2@C_{80}$ in $Sc_3N@C_{80}$ (1 mol%) are shown in Figure S3. The results are similar to those of $Sc_3C_2@C_{80}$ in toluene. The difference is that the critical temperature in EPR signal intensity curve of $Sc_3C_2@C_{80}$ in $Sc_3N@C_{80}$ is enhanced due to the complete immobilization of carbon cage. Obviously, the slow motion (Sc_3C_2 moiety in C_{80} cage) can

also occur even if the carbon cage is completely immobilized when $Sc_3C_2@C_{80}$ is in solid state. This can indirectly illustrate that the decreased EPR signal of $Sc_3C_2@C_{80}$ in MOF-177 with decreasing temperature originates from the special host-guest interaction and the shrinkage of MOF-177.

Temperature-dependent EPR spectra and temperature-dependent EPR peaks intensity of 4-hydroxy-2,2,6,6-tetramethyl-piperidinooxy in solid and in toluene solution are shown in Figure S4. The changes of intensities for EPR spectra clearly illustrate the possibility of comparing directly the intensities of the EPR spectra taken at different temperatures and can deduce conclusions on this basis.

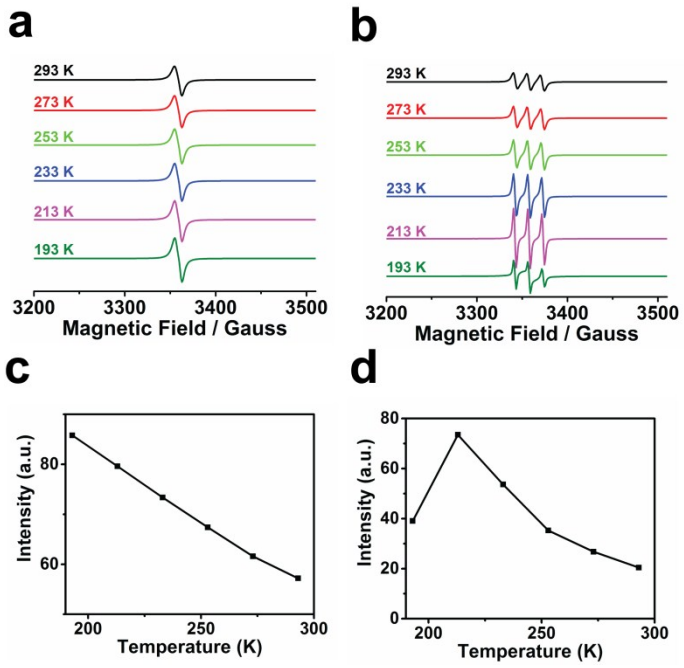

Figure S4. Temperature-dependent EPR spectra of 4-hydroxy-2,2,6,6-tetramethyl-piperidinooxy in solid (a) and in toluene solution (b). Temperature-dependent EPR peaks

intensity of 4-hydroxy-2,2,6,6-tetramethyl-piperidinooxy in solid (c) and in toluene solution (d).

The simulated EPR spectra of $Sc_3C_2@C_{80}$ in toluene solution at 293 K and 193 K are shown in Figure S5. The Scandium hyperfine coupling constants and g-values used: 293 K : g = 1.9960, A = 6.28 G; 193 K : g = 1.9960, A = 6.49 G. For $Sc_3C_2@C_{80}$@MOF-177, the smilulation of EPR spectra at 293 K is only got due to many nuclei in the system.

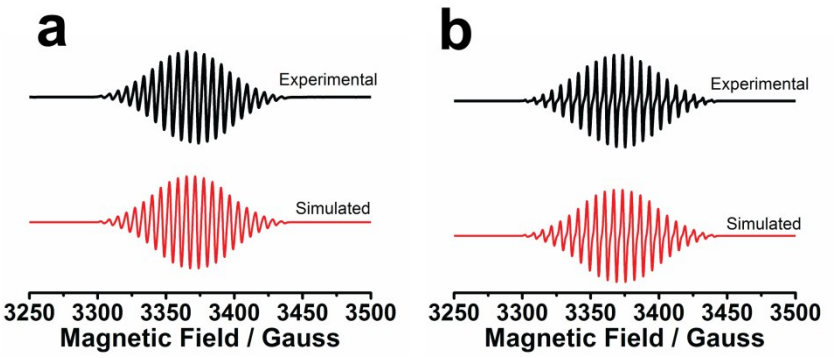

Figure S5. The experimental (black) and simulated (red) EPR spectra of $Sc_3C_2@C_{80}$ in toluene solution at 293 K (a), 193 K (b).

Time-dependent EPR peaks intensity of $Sc_3C_2@C_{80}$@MOF-177 (a) and $Sc_3C_2@C_{80}$ in $Sc_3N@C_{80}$ (b) at 2.13×10^4 Pa are shown in Figure S6. The EPR peaks intensity of them don't greatly change at subatmospheric pressure.

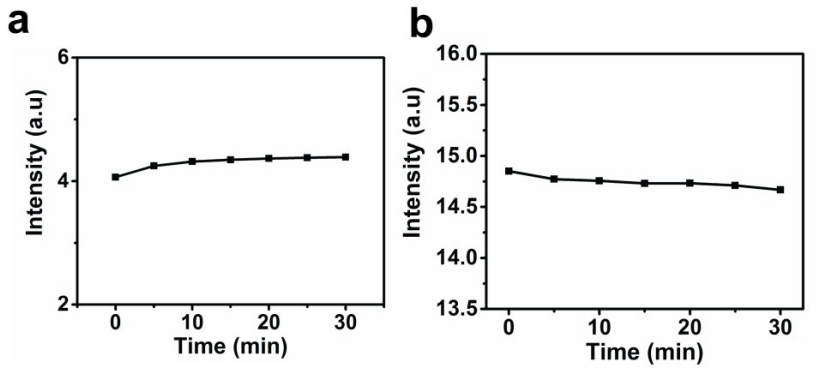

Figure S6. Time-dependent EPR peaks intensity of $Sc_3C_2@C_{80}$@MOF-177 (a) and time-dependent EPR peaks intensity of $Sc_3C_2@C_{80}$ in $Sc_3N@C_{80}$ (1 mol%) (b) at 2.13×10^4 Pa.

The line widths of $Sc_3C_2@C_{80}$@MOF-177 in the first integral of the EPR spectra are gradually decreased with decreasing pressure, indicating the weak host-guest interaction and more free motion of $Sc_3C_2@C_{80}$.

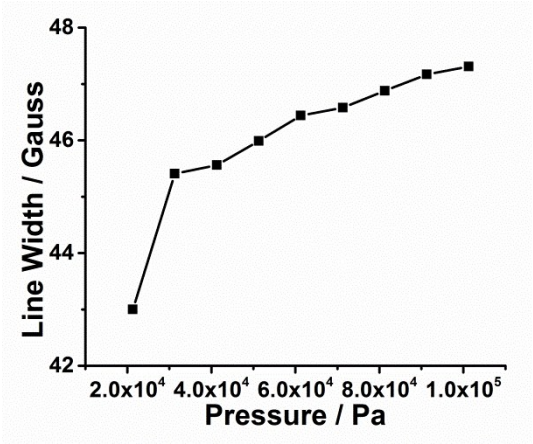

Figure S7. The line widths of $Sc_3C_2@C_{80}$@MOF-177 in the first integral of the EPR spectra.

The experimental and fitted line width of the EPR spectra for $Sc_3C_2@C_{80}$ in MOF-177 (a) and in toluene (b) at 293 K plotted against quantum number M_I of the Sc_3 nuclear magnetic moment is shown in Figure S8. Obviously, the plot shows a parabolic

dependence on m_I, and the slope of the plots becomes steeper at lower temperature (Figure 5e). From the fitted curve according to Kivelson's equation[3, 4], we could obtain the value of k_i parameters for $Sc_3C_2@C_{80}$ in MOF-177 at 293 K, 253 K and 193 K (Table S1). k_0 is related not only to the rotational correlation time but also to dipole-dipole interactions (the exchange interactions can be neglected due to the low concentration of $Sc_3C_2@C_{80}$ in MOF-177 pores and in toluene). We also obtained the k_0 parameters for $Sc_3C_2@C_{80}$ in toluene (other k_i parameters are so small and can be neglected), indicating that the changed line width for $Sc_3C_2@C_{80}$ in toluene is attributed to the rotational correlation time and dipole-dipole interactions. The value of k_0 are 2.34 at 293 K, 1.76 at 253 K and 1.76 at 193 K. In theory, the rotational correlation time τ_c can be extracted from k_1, which is independent of exchange and dipole-dipole interactions.

$$k_1 \propto \tau_c (a_{aniso})(g_{aniso})$$

where g_{aniso} and a_{aniso} are the terms denoting the anisotropic **g** tensor and the anisotropic hyperfine tensor, respectively. However, both the viscosity (η) of MOF-177 g_{aniso} and a_{aniso} are unknown. Because of lack of prior knowledge, there is no possibility of deducing g and hyperfine tensor anisotropy as well as rotational correlation time from the fitted data.

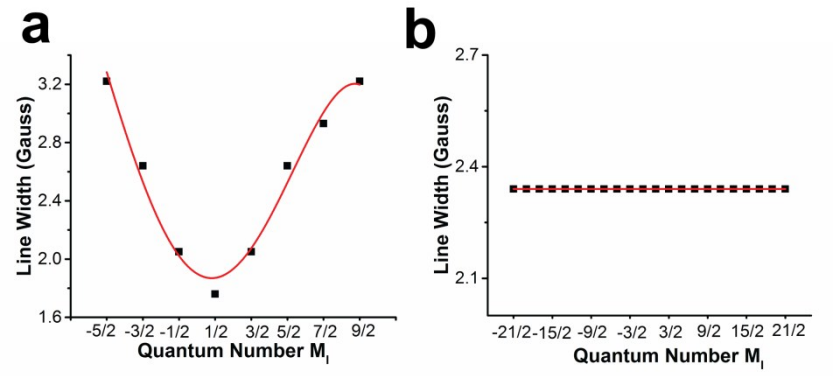

Figure S8. Experimental (black squares) and fitted (red line) line width of the EPR spectra for $Sc_3C_2@C_{80}$ in MOF-177 (a) and in toluene (b) at 293 K plotted against quantum number M_I of the Sc_3 nuclear magnetic moment.

Table S1. Experimental k_i parameters for $Sc_3C_2@C_{80}$ in MOF-177 at 293 K, 253 K and 193 K.

	k_0	k_1	k_2	k_4
293 K	1.8996	-0.1515	0.1888	-0.0045
253 K	2.0152	-0.1068	0.2451	-0.0095
193 K	2.2786	-0.1170	0.2315	-0.0066

3. EDS measurements

EDS file of $Sc_3C_2@C_{80}$@MOF-177 at 293 K is shown in Figure S8. The characteristic

peak of scandium indicates that $Sc_3C_2@C_{80}$ guests are encapsulated into the pores of MOF-177.

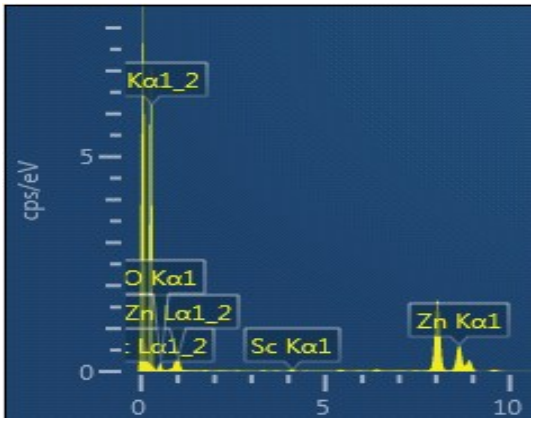

Figure S9. EDS file of $Sc_3C_2@C_{80}$@MOF-177 complex at 293 K.

4. Geometries of MOF-177

The $Sc_3C_2@C_{80}$ and $Sc_3C_2@C_{80}$@MOF-177 unit were firstly optimized using original pm6 and b3lyp/3-21g* to speed up the computational process using the Gaussian 09 quantum chemical program package,[5] and then accomplished by using the Dmol3 code[6, 7] with the generalized gradient approximation (GGA) functional of Perdew, Burke, and Ernzerhof(PBE)[8] using the materials studio 7.0 software. For open-shell systems, the spin-unrestricted algorithms were used. All-electron double-numerical basis set with polarization functions (DNP) was applied for all atoms. To take into account relativistic effects, the all-electron scalar relativistic method utilizing the Douglas-Kroll-Hess (DKH) Hamiltonian was chosen.[9] As shown below, one of the two nearest ligands from opposite sides is marked with purple.

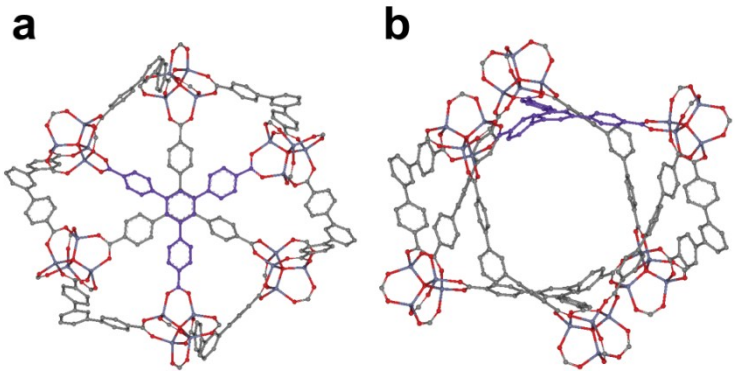

Figure S10. DFT-calculated geometries of MOF-177 along the direction of two nearest ligands from opposite sides (a) along the direction that perpendicular to the nearest ligands from opposite sides (b). Color code: light blue, Zn; light purple, O; red, C; gray. H atoms and guest molecules are omitted for clarity.

5. Single X-ray diffraction measurements

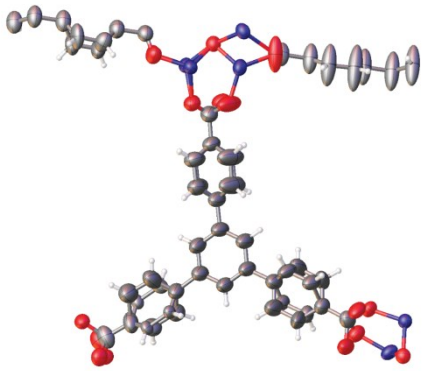

Figure S11. Ortep representation of the symmetric unit in MOF-177 at 193 K (Zn, purple; C, gray; O, red; H atoms are omitted for clarity).

Single X-ray diffraction (XRD) of MOF-177 was performed with Cu Kα radiation on MM007HF Saturn724+ at 193 K.

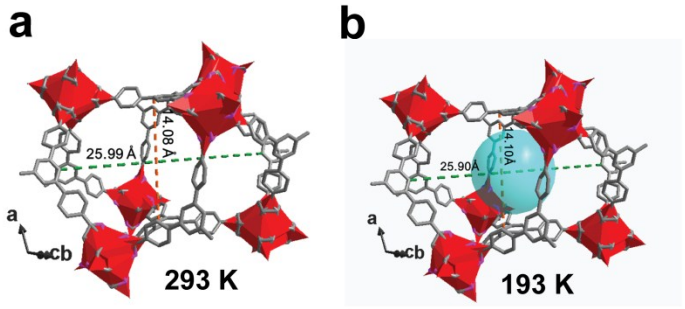

Figure S12. The parameters of cage-shaped pores in MOF-177 crystals at 293 K (a) and 193 K (b). The gray parts, ligand; the red polyhedral, Zn-O cluster. H atoms and solvent molecules are omitted for clarity.

The unit cell volume of MOF-177 decreases from 36020.3 $Å^3$ to 35584.7 $Å^3$ along with decreasing temperature (Table S1), illustrating the slight shrink of the MOF-177 crystal under low temperatures. The shortest distance of cage-shaped pore in MOF-177 changes from 14.10 to 14.18 Å, and the width of that changes from 25.99 to 25.90 Å with decreasing temperature (Figure S11). The reduced width of MOF-177 cage-shaped pore would force $Sc_3C_2@C_{80}$ molecule to the center of pores in MOF-177. At this point, DFT-calculation has been disclosed the strong host-guest interaction, which may finally hinder the motion of $Sc_3C_2@C_{80}$. In general, the slight shrinkage of MOF-177 with decreasing temperature may intensify the host-guest interaction between $Sc_3C_2@C_{80}$ and MOF-177 and hinder the motion of $Sc_3C_2@C_{80}$, leading to the changes of paramagnetic properties of $Sc_3C_2@C_{80}$.

Table S2.Crystal data and structure refinement for MOF-177 at 293 K[10] and 193 K.

Temperature	293K	193K
Empirical formula	$C_{54}H_{30}O_{13}Zn_4$	$C_{54}H_{30}O_{13}Zn_4$
Formula weight	1148.26	1148.27
Temperature/K	293.15	193.01(10)
Crystal system	Trigonal	Trigonal
Space group	P -31c	P-31c
a/Å	37.166(5)	37.0345(7)
b/Å	37.166(5)	37.0345(7)
c/Å	30.111(6)	29.9585(6)
α/°	90	90
β/°	90	90
γ/°	120	120
Volume/Å^3	36021(13)	35584.7(15)
Z	8	7.99992
ρ_{calc}g/cm^3	0.423	0.429
μ/mm^{-1}	0.544	0.764
F(000)	4624	4624.0
Crystal size/mm^3	0.23 x 0.16 x 0.14	0.20 x 0.13 x 0.10
Radiation	CuKα (λ = 1.54184)	CuKα (λ = 1.54184)
2Θ range for data collection/°	1.266 to 49.998	7.292 to 143.362
Index ranges	-43<=h<=43, -44<=k<=29, -30<=l<=35	-28 ≤ h ≤ 45, -45 ≤ k ≤ 43, -34 ≤ l ≤ 36
Reflections collected	123302	84265
Independent reflections	21170 [R_{int} = 0.1014]	22751 [R_{int} = 0.0450, R_{sigma} = 0.0370]

Data/restraints/parameters	21170 / 1473 / 674	22751/1/598
Goodness-of-fit on F^2	1.641	1.041
Final R indexes [I>=2σ (I)]	R_1 = 0.1282, wR_2 = 0.3091	R_1 = 0.0639, wR_2 = 0.1940
Final R indexes [all data]	R_1 = 0.1512, wR_2 = 0.3226	R_1 = 0.0876, wR_2 = 0.2159
Largest diff. peak/hole / e $Å^{-3}$	0.469/-0.331	0.55/-0.31

4. References

(1) H. W. Kroto, J. R. Heath, S. C. O'Brien, R. F. Curl and R. E. Smalley, *Nature.*, 1985, **318**, 162-163.

(2) H. Shinohara, H. Sato, M. Ohkohchi, Y. Ando, T. Kodama, T. Shida, T. Kato and Y. Saito, *Nature.*, 1992, **357**, 52-54.

(3) R. Wilson and D. Kivelson, *J. Chem. Phys.*, 1966, **44**, 154-168.

(4) P. Jakes, A. Gembus, K. P. Dinse and K. Hata, *J. Chem. Phys.*, 2008, **128**, 052306.

(5) Frisch, M.; Trucks, G.; Schlegel, H.; Scuseria, G.; Robb, M.; Cheeseman, J.; Scalmani, G.; Barone, V.; Mennucci, B.; Petersson, G. **2009**.

(6) Delley, B. *J. Chem. Phys.,* 1990, ***92***, 508.

(7) Delley, B. *J. Chem. Phys.,* 2000, ***113***, 7756.

(8) Perdew, J. P.; Burke, K.; Ernzerhof, M. *Phys. Rev. Lett.,* 1996, ***77***, 3865.

(9) Douglas, M.; Kroll, N. M. *N. M. Ann. Phys.* 1974, **(1)**, 89-155.

(10) Y. Feng, T. Wang, Y. Li, J. Li, J. Wu, B. Wu, L. Jiang and C. Wang, *J. Am. Chem. Soc.*, 2015, **137**, 15055-15060.